JOTCS A
Journal of the Turkish Chemical Society
Section: A
Chemistry
TURKISH CHEMICAL SOCIETY

Enhancing Biogas Production with The Addition of Nano-catalysts

Fatih Mehmet Emen[1*], Aslıhan Cesur Turgut[2], Şevkinaz Doğan[3]

[1]Burdur Mehmet Akif Ersoy University, Department of Chemistry, Burdur, 15003, Türkiye.
[2]Burdur Mehmet Akif Ersoy University, Department of Plant and Animal Production, Burdur Vocational School of Food, Agriculture and Livestock, Burdur, 15030, Turkiye.
[3]Burdur Mehmet Akif Ersoy University, Department of Fundamentals of Nursing, Faculty of Health Sciences, Burdur, 15030, Turkiye.

Abstract: The province of Burdur is at the forefront of the livestock industry, especially with dairy cattle. it is a necessity for Burdur province to use animal manure, convert it into methane gas, and use it as fuel. In this study, a laboratory-scale biodigester was set up to produce biogas from cattle feces taken from Burdur Mehmet Akif Ersoy University Cattle Farm. γ-Fe_2O_3, meso-Fe_2O_3, and meso-Co_3O_4 nanoparticles (NPs) were synthesized and used as catalysts for biogas production. Structural characterizations of catalysts were carried out via FT-IR and XRD techniques. The TEM was used to investigate particle size distributions and morphology. The average particle sizes of the nanoparticles were determined to be in the range of 20-165 nm. The bio-digester was kept at a constant temperature of 35 °C for 20 days. It has been determined that the obtained biogas has a high methane content of 83–86%. The biogas volume was obtained to be 1.360 L/kg for γ-Fe_2O_3, 1.390 L/kg for meso-Fe_2O_3, and 625-1.250 L/kg for Co_3O_4.

Keywords: Biogas, Cattle Manure, Digester, Methane, hydrothermal method, Fe_2O_3, Co_2O_3.

Submitted: September 28, 2023. **Accepted:** February 18, 2024.

Cite this: Emen FM, Cesur Turgut A, Doğan Ş. Enhancing Biogas Production with The Addition of Nano-catalysts. JOTCSA. 2024;11(2):643-54.

DOI: https://doi.org/10.18596/jotcsa.1368040

***Corresponding author's E-mail:** femen@mehmetakif.edu.tr

1. INTRODUCTION

Renewable energy helps solve environmental problems and support sustainable development. Renewable energy sources reduce climate change by emitting little greenhouse gas (1). They boost energy security by diversifying the energy mix and minimizing fossil fuel imports. Renewable energies improve air quality and health (2). They also boost economic growth, investment, and job creation (3). Renewable energy technology advances improves efficiency, and lowers costs, making it more accessible and profitable. Renewable energies are crucial to the climate and ecological goals of the Green Deal, such as the European Green Deal. By 2050, it wants to make Europe the first climate-neutral continent by focusing on renewable energy and energy efficiency. The Green Deal encourages renewable energy use to reduce greenhouse gas emissions and boost economic growth. It supports renewable energy development and implementation through policies, financing, and research. Countries can fight climate change and promote sustainability by supporting the Green Deal (4). Biomass energy is a term that encompasses bioenergy and biofuels. Bioenergy refers to solid biomass used for domestic uses (heating, cooking) and industrial applications (heat and power). Biofuels mainly refer to liquid biofuels (biodiesel and bioethanol) used in road transportation but also include biogas. Biomass energy is a renewable resource that has the potential to contribute significantly to the world's energy needs. Anaerobic digestion (AD) of agricultural waste, food waste, and sewage sludge produces biogas. Waste management, renewable energy generation, methane emission reduction, and nutrient recycling are its benefits. Methane in biogas is used to generate energy. Electricity, heating, and cooking can be made from biogas. The energy performance of biogas production can be assessed using parasitic energy demand, biogas utilization efficiency, and energy output relative to feedstock solid mass. These indicators reveal biogas plant energy efficiency and performance. Producing biogas from organic waste has many benefits. Organic waste serves as a valuable substrate for anaerobic digestion, a natural process mediated by a diverse array of microorganisms. Anaerobic digestion

converts organic residues into biogas, and volatile fatty acids, which hold potential as clean energy sources. The anaerobic digestion process comprises four interconnected steps wherein microorganisms in each step sequentially convert substrates for utilization by subsequent microbial communities (5-7). It is a complex process in which a diverse consortium of microorganisms uses organic waste as a substrate to initiate an integrated and multifaceted cascade of biochemical reactions in single-stage batch reactors, including hydrolysis, acidogenesis, acetogenesis, and methanogenesis. After this procedure, biogas—an infinite source of renewable energy that can be used for thermal applications—is produced (8). Biogas installations number 132,000 worldwide, excluding 50 million micro-scale digesters (9). Nanoscale particles or structures make up nanocatalysts. These catalysts have unique features and advantages due to their compact size and high surface area-to-volume ratio. In recent years, nanocatalysis has advanced, with many types of nanocatalysts being studied for various uses (10). In a research pressmud as a substrate for anaerobic digestion with a CuO/Cu_2O nanocatalyst to improve biogas. The aqueous extract of PM and SCB used as a reducing agent was used to make CuO/Cu_2O nanocatalyst. Using 1.0 % CuO/Cu_2O nanocatalyst in the AD process, a total biogas of 224.7 mL CH_4 /g VS was reported after 42 days (11). In a different study, water is divided electrochemically using a nanocatalyst and an external energy source to produce hydrogen and oxygen. Copper (Cu) based nanostructures have been found to have an impact on the stability, immobilization, and recovery of enzymes among a variety of investigated nanomaterials (12). Furthermore, the inclusion of Cu-based nanomaterials may have improved the CAZymes' (carbohydrate-active enzymes) functional activity, which raises the efficiency of cellulose degradation during the enzymatic hydrolysis reaction (13). Platinum-based nanocatalysts can boost water-splitting efficiency. These nanocatalysts increase electrochemical reaction activity and energy conversion by providing many active sites. Other research examines nanocatalysts in organic processes. Gold nanoparticles have been widely investigated as organic transformation catalysts. Gold nanoparticles promote selective and sustained reactions due to their unique electrical and structural features. Energy applications like fuel cells use nanocatalysts. Platinum-based nanocatalysts are frequently used in fuel cell technologies due to their excellent catalytic activity and stability. These nanocatalysts aid electrochemical reactions that convert chemical energy to electricity. Research has also focused on nanocatalyst synthesis and design. Various approaches have been developed to alter nanocatalyst size, shape, and composition for customized characteristics and better catalytic performance. Support materials like carbon nanotubes or metal oxides can improve nanocatalyst stability and reactivity. Nanocatalysts' small size and high surface area-to-volume ratio allow them to improve catalytic processes. They are promising for water splitting, chemical processes, fuel cells, and more. Nanocatalysis research could improve energy generation, environmental cleanup, and chemical synthesis (14-18). Nanocatalysts can contribute to the production efficiency of biogas and other biofuels. Nanocatalysts accelerate the degradation of organic waste and the creation of methane, the main component of biogas. They boost catalytic activity, selectivity, and stability. Bharathi et al. (2022) (19) employed iron oxide nanoparticles to boost bacterial growth, minimize retention time, and produce biogas from food waste. Nanocatalysts' high surface area and reactivity help convert organic waste into biogas. They can boost conversion efficiency, product yield, and byproduct reduction. Nanocatalysts can be optimized for specific processes and feedstocks by changing size, content, and structure. However, nanocatalysts for biogas production are still being studied. Further research is needed on catalyst production, loading optimization, and nanocatalyst-microbial community interactions. Nanocatalysts' environmental impact and cost-effectiveness in large-scale biogas generation should also be evaluated (20).

In this study, it was aimed to examine the contribution of magnetic nanoparticles to the production of biogas from cattle manure. Few studies are using mesoporous Fe_2O_3. However, studies on biogas production using mesoporous Co_3O_4 as a catalyst have not been found. For this purpose, γ-Fe_2O_3, meso-Fe_2O_3, and meso-Co_3O_4 NPs were synthesized and characterized. The laboratory-scale biodigester was designed and set up to produce biogas from cattle feces taken from Burdur Mehmet Akif Ersoy University Cattle Farm.

2. EXPERIMENTAL SECTION

2.1. Materials

In the synthesis of metal oxide NPs, iron (III) chloride hexahydrate ($FeCl_3.6H_2O$, Merck), cobalt (III) chloride hexahydrate ($CoCl_3.6H_2O$), ethylene glycol (99%, Merck), polyethylene glycol (PEG, 1000, Merck), sodium acetate trihydrate ($CH_3COONa.3H_2O$, Sigma Aldrich), and sodium hydroxide (NaOH, Merck) were used.

2.2. Instrumentations

A Bruker AXS-D8 advanced model instrument was used in X-ray powder diffraction (XRD) analyses performed to elucidate the structures of the synthesized metal oxide nanoparticles. X-ray diffraction (XRD) studies were performed using a nickel filter (0.2 mm) and copper tube (Cu-Kα) radiation at 40 kV. XRD data were recorded at a scan step of 0.02° and angles of $10° \leq \theta \leq 90°$. FT-IR spectra were recorded in the range of 4000-400 cm^{-1} using the Shimadzu IRTracer-100 spectrometer. A JEOL-JEM-1400 PLUS model Transmission Electron Microscopy (TEM) system was used for particle size and morphological examinations. 7890A GC 5975C MS gas chromatography system combined with the Agilent 7697A Headspace was used to determine the percentage of methane in the biogas content. The headspace vial which contains activated carbon was used for sampling.

2.3. Method

2.3.1. Preparation of nanoparticles

Generally, in the hydrothermal synthesis method, metal oxide nanoparticles are synthesized in an aqueous solution of metal salts. The resulting oxide is obtained from water as a reservoir. However, in this study, the water source during the reaction is $FeCl_3.6H_2O$ and $CoCl_3.6H_2O$. Additionally, polyethylene glycol (PEG) added to this reaction is used as an oxidant, surfactant, and anti-aggregation agent. Thus, it prevents particle accumulation and ensures the formation of high surface area Fe_2O_3 and Co_3O_4.

Synthesis of γ-Fe_2O_3 nanoparticles

The hydrothermal synthesis method was used to synthesize γ-Fe_2O_3 nanoparticles (21) $FeCl_3.6H_2O$ (0.99 g) was mixed with ethylene glycol (40mL) until dissolved. Sodium acetate (CH_3COONa) (3.6 g) and polyethylene glycol (PEG-1000) (1 g) were added and mixed for 45 minutes. The mixture was transferred into a Teflon-lined (50 mL) stainless steel autoclave and heated in an oven at 190°C for 5 hours. The resulting black product was collected by decantation, and the product was washed several times with ethanol. Then it was dried at 70°C for 12 hours.

Synthesis of mesoporous Co_3O_4 nanoparticles

Mesoporous Co_3O_4 was synthesized by modifying the method given in the literature (22). $CoCl_3.6H_2O$ (0.99 g) was dissolved in 40 mL of Ethylene glycol. Sodium acetate (CH_3COONa) (3.6 g) and polyethylene glycol (PEG-1000) (1 g) were added to the first solution and mixed for 45 minutes. The mixture was transferred into a Teflon-lined (50mL) stainless steel autoclave and heated in an oven at 190 °C for 5 hours. The resulting black product was collected by decantation, and the product was washed several times with ethanol. Then it was dried at 70 °C for 12 hours.

Preparation of mesoporous Fe_2O_3 nanoparticles

Mesoporous Co_3O_4 was synthesized by modifying the method given in the literature (23). 0.5 g of hexadecyltrimethylammonium bromide (CTAB) was solved in 96 mL of deionized water. Then 34 mL of ethanol and 10 mL of NH_3 were added and mixed for 5 minutes. Finally, 2 mL of tetraethylorthosilicate (TEOS) was added and stirred at room temperature for 3 hours. Then, it was heated in a muffle furnace at 550 °C for 10 hours. MCM-41 was immersed in the previously prepared 1.0 M of $Fe(NO_3)_3$ solution. MCM-41-Fe_2O_3 was heated again at 550 °C and then treated with a 10 M NaOH solution to remove SiO_2. The obtained mesoporous Fe_2O_3 nanoparticles were washed with deionized water and dried.

2.3.2. Experimental design of AD process

Collection of samples

Animal feces with urine were collected from the slurry pit at Burdur Mehmet Akif Ersoy University (MAKU) Cattle Farm and used for the AD process without delay. The pH value was checked before biogas production.

Biogas production in a laboratory-scale biodigester system

A laboratory-scale biodigester (total volume is 5.0 L) with a 1.0 L working volume was used (Figure 1). The outer wall of the biodigester, which was developed for this study, contains a water jacket, and the ambient temperature is kept under control by keeping the water temperature constant with a heater. In light of all these explanations, the working temperature was determined to be 35 °C, and the temperature was kept constant during fermentation. 500 g of feces were taken and diluted with water. The final %TS value of the mixture in the bioreactor was set up as 20% for each trial and three replicates were performed. The pH value of the feces used in the study was 7.35, and the temperature value was 16.5 °C. Nanocatalysts were added to the bioreactor and mixed at a constant temperature for 20 days. To disrupt microbial cells and increase the biodegradation efficiency of the feces, the aqueous feces were mixed at a speed of 6 rpm per minute with the propeller mixer mounted on the system under mesophilic conditions (35 °C) so as not to precipitate. This phase lasted 20 days. The catalyst amounts and waiting times used were taken from the literature, and the study was completed (24). 0.3 g/L catalyst was used in each bioreactor.

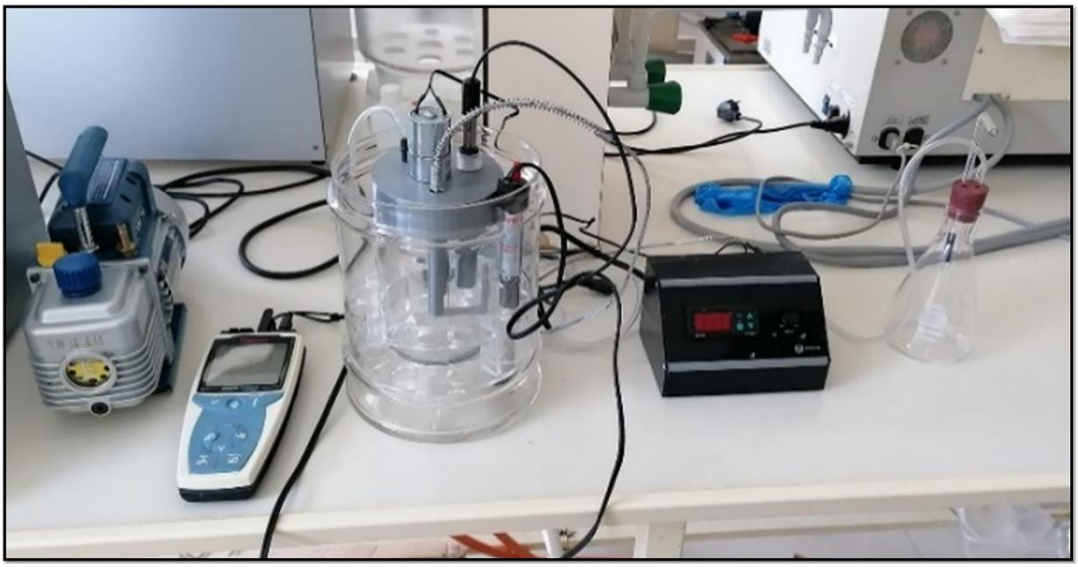

Figure 1: Biogas digester system.

A headspace vial which contains activated carbon was used for sampling. In the Headspace system, the gases are released from activated carbon and they were analyzed by Headspace-GC-MS. The amount of methane in the resulting biogas was analyzed using the 7890A GC 5975C MS gas chromatography system combined with the Agilent 7697A Headspace. The analysis method is detailed below (25):

Column temperature program: After waiting at 35°C for 5 minutes, it reaches 150 °C with an increase of 5 °C per minute and is kept at this temperature for 5 minutes. Detector and injector temperatures: 200 °C and 180 °C, Flow Rate: 25 psi (He), Needle: 90 °C, transfer line: 120 °C, Vial oven: 85 °C, Thermostat time: 5 minutes, pressurize time: 0.5 minutes, inject time: 0.08 minutes, Withdraw time: 0.5 minutes.

The amount of methane in the biogas content obtained without catalyst and with catalyst (γ-Fe_2O_3, Meso-Fe_2O_3, and Meso-Co_3O_4) in the biodigester was calculated from the peak area using the gas chromatogram. In addition, the MS detector connected to the system was used to determine which compound the relevant peak belonged to. A representative gas chromatogram is given in Figure 2.

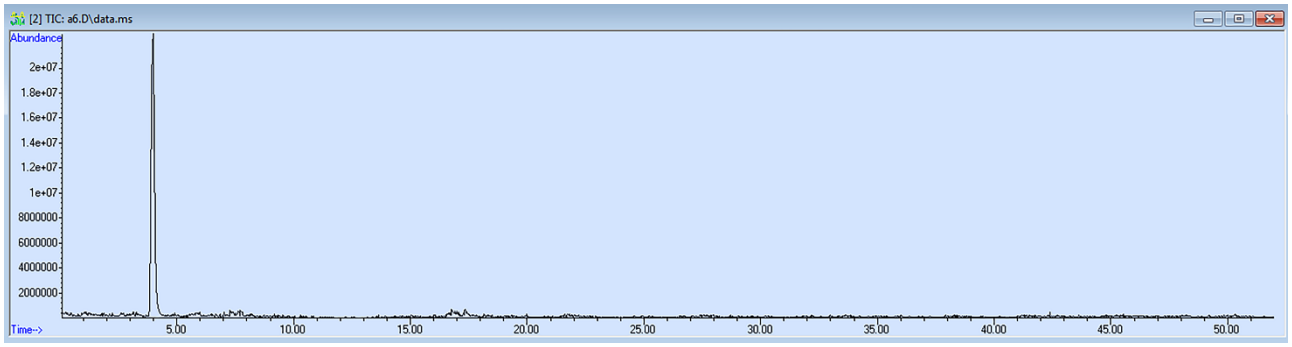

Figure 2: Gas chromatogram showing methane content in biogas.

2.4.3. Chemical characterization

The amount of dry matter, volatile solids, crude protein, and crude oil was determined in the collected biomass samples (26). Feces samples were dried at 105 °C for 24 hours and the amount of dry matter was calculated. After the dry matter was digested at 550 °C for 3 hours, the amount of Volatile solid was determined by taking the difference between the dry matter and ash components. Total Kjeldahl nitrogen (TKN) composition was determined according to the standard method (27), and crude protein nitrogen composition was determined by multiplying the TKN value by 6.25. The crude oil was determined by dissolving the substrates in diethyl ether according to the Soxhlet method (28).

3. RESULTS AND DISCUSSION

3.1. Characterization of Nanoparticles

3.1.1. XRD results of the nanoparticles

XRD powder patterns of the nanoparticles were recorded in the range of 10-90°. The XRD powder pattern of γ-Fe_2O_3 nanoparticles is given in Figure 3. The peaks with (206), (119), (0012), (1115), and (4012) hkl values correspond to γ-Fe_2O_3 nanoparticles which are in the maghemite structure formed (PDF card no: 00-025-1402). These results are compatible with the literature (29). The crystal system of γ-Fe_2O_3 is tetragonal, the space group is P43212(96) and the cell parameters are a=b=8.34 Å, c=25.02 Å, α=β=ɣ=900, V=140.28 $Å^3$. The fact that no impurity peaks were found in the powder pattern shows that γ-Fe_2O_3 was synthesized as a single phase.

The XRD powder pattern of mesoporous Fe_2O_3 nanoparticles is given in Figure 4. In the XRD pattern, the peaks obtained with (306), (134), (128), (220), (1010), (300), (214), (018), (116), (024), (113), (110), (104) and (012) hkl values. These results indicate that Fe_2O_3 is formed in the hematite structure (PDF Card no: 00-033-0664) (23). Fe_2O_3 was obtained in a rhombohedral crystal system with an R-3c (167) space group. Cell parameters are a=b= 5.03560 Å, c= 13.74890 Å, α=β=ɣ=900, V= 301.93 $Å^3$. There are no impurity peaks were found in the powder pattern showing that mesoporous-Fe_2O_3 was synthesized as a single phase.

The XRD powder pattern of mesoporous Co_3O_4 NPs is given in Figure 5. All peaks in the XRD pattern show that the Co_3O_4 structure (PDF card no: 00-042-1467) is formed in pure form and does not contain any impurity peaks (22). The crystal system of Co_3O_4 is cubic, the space group is Fd-3m (227) and the cell parameters are a=b=c= 8.03730 Å, α=β=ɣ=90.0, V=524.24 $Å^3$.

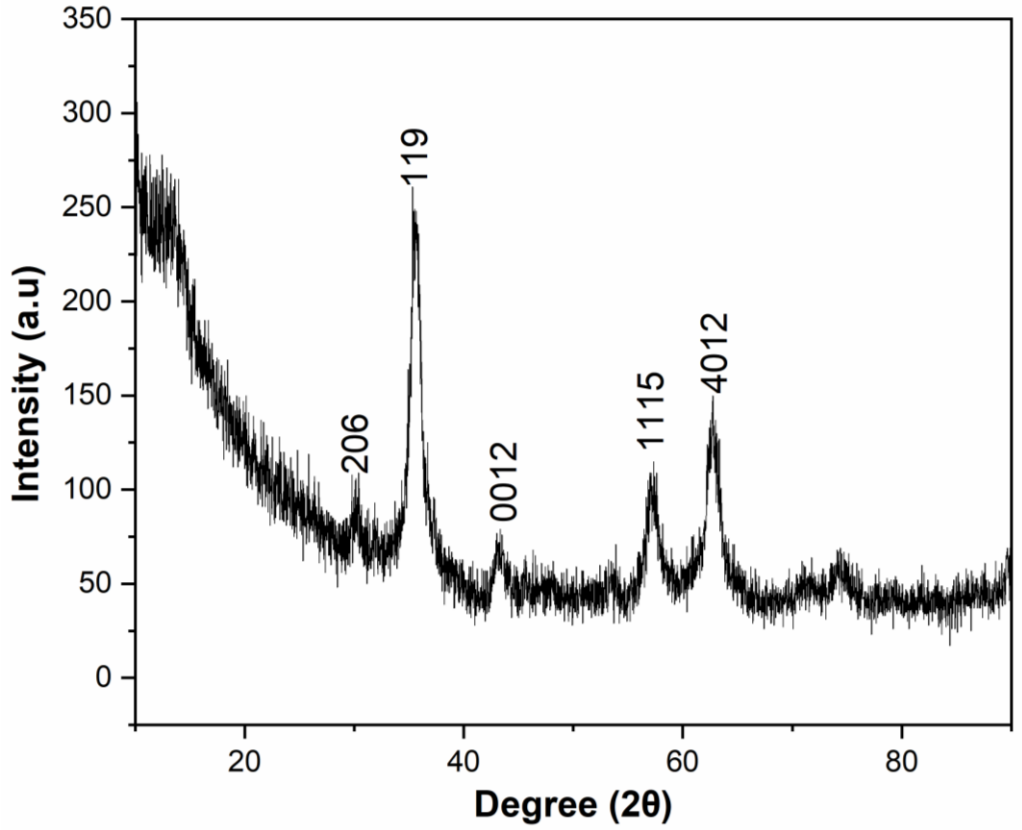

Figure 3: XRD powder pattern of γ-Fe_2O_3 nanoparticles.

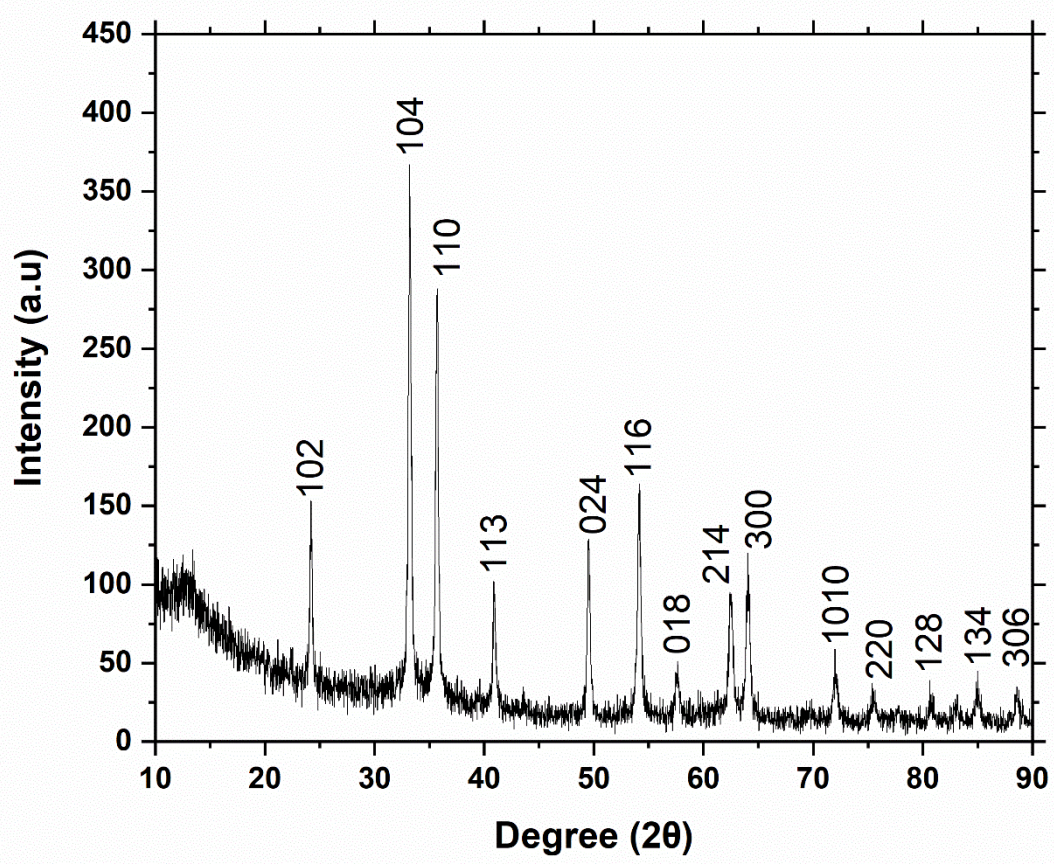

Figure 4: XRD powder pattern of mesoporous Fe_2O_3 nanoparticles.

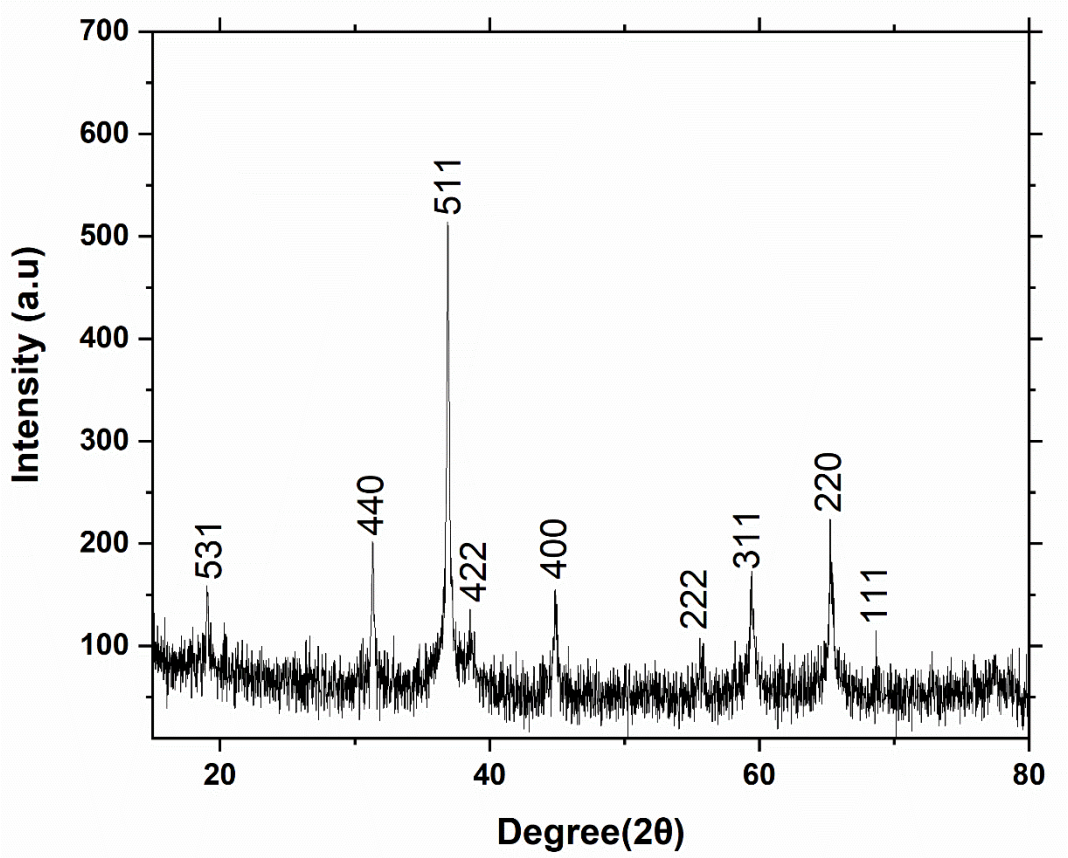

Figure 5: XRD powder pattern of meso-Co_3O_4 NPs.

3.1.2. FT-IR results of the nanoparticles

The FTIR spectra of the synthesized nanoparticles were taken in the range of 4000-400 cm^{-1} using KBr pellets. The FT-IR spectra of γ-Fe_2O_3 and mesoporous-Fe_2O_3 nanoparticles are given in Figures 6 and 7. FT-IR spectra of γ-Fe_2O_3 and mesoporous-Fe_2O_3 nanoparticles are identical because the vibrations of the same elements are analyzed. Three peaks were observed in the FT-IR spectrum of the nanoparticles at 543, 1637, and 3428 cm^{-1}. The peak observed at 543 cm^{-1} corresponds to the symmetric vibrations of Fe-O bonds. Water molecules are absorbed on the surfaces of Fe_2O_3 nanoparticles (30). Therefore, the peaks observed at 3428 and 1630 cm^{-1} in the FTIR spectrum belong to the stretching and bending vibrations of water molecules, respectively.

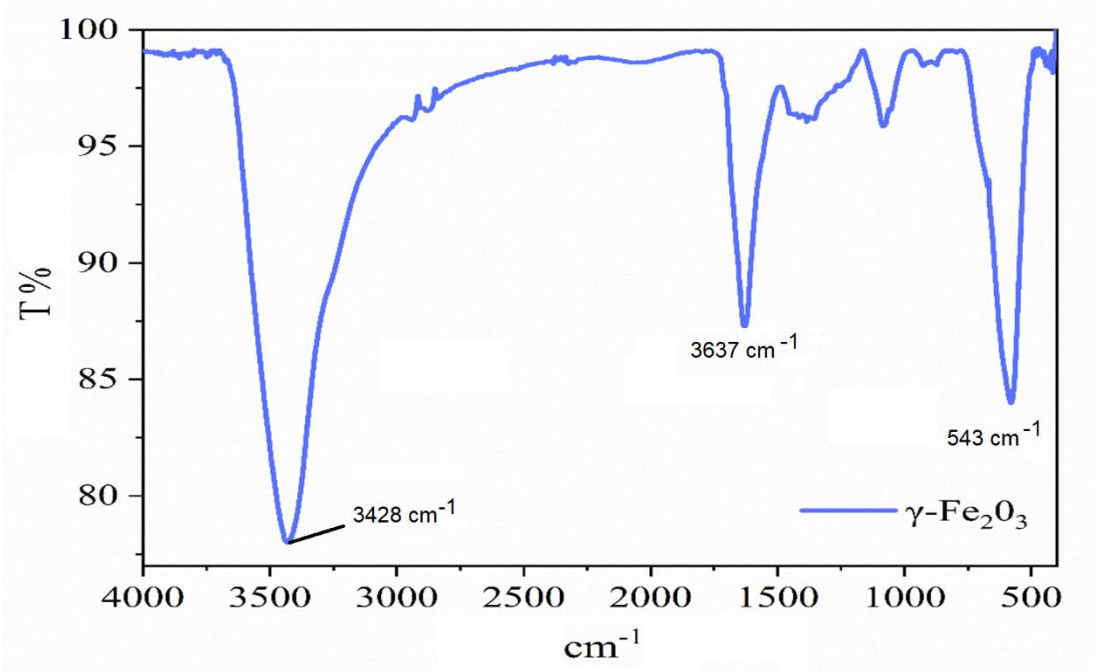

Figure 6: FTIR spectrum of γ-Fe_2O_3 NPs.

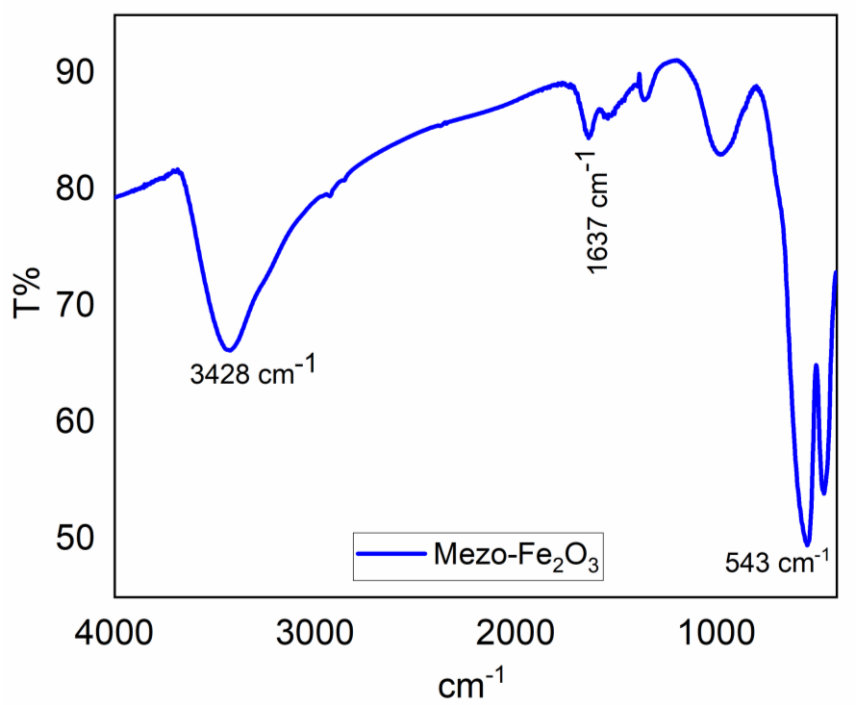

Figure 7: FTIR spectrum of meso-Fe_2O_3 NPs.

FT-IR spectrum of mesoporous Co_3O_4 NPs is given in Figure 8. Water molecules are absorbed on the surfaces of Co_3O_4 nanoparticles. Therefore, the peaks observed at 3430 and 1635 cm^{-1} in the FTIR spectrum belong to the stretching and bending vibrations of water molecules, respectively. The broad peaks in the absorption bands around 673 and 580 cm^{-1} are due to the stretching vibration of the metal-oxygen bond and the IR absorptions of Co_3O_4. The presence of this band indicates that cobalt is in a hexagonal oxygen octahedral environment and thus Co_3O_4 is formed (31).

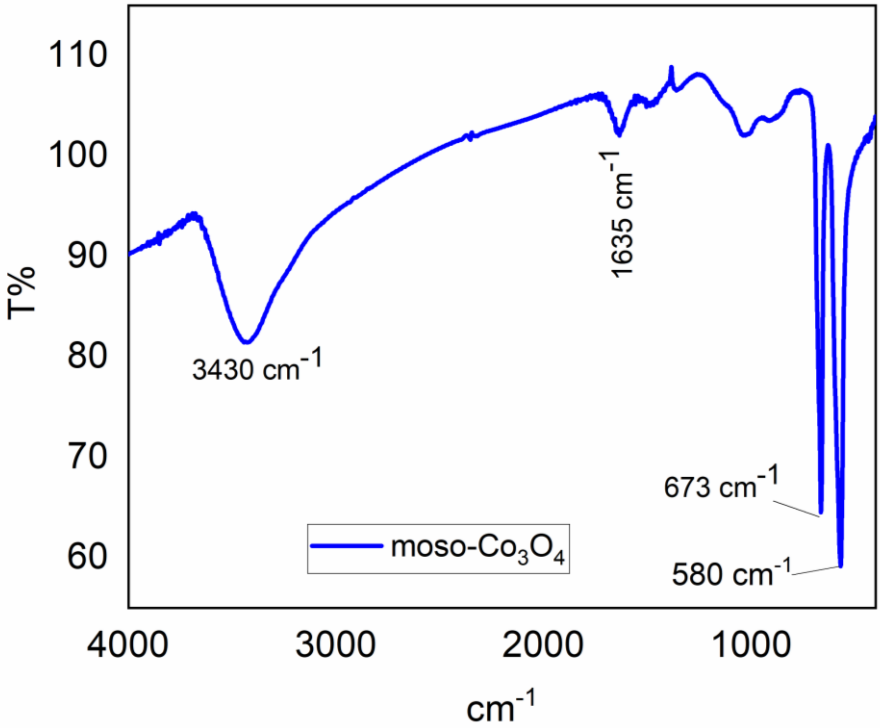

Figure 8: FTIR spectrum of meso-Co_3O_4 NPs.

3.1.3. Transmission Electron Microscope (TEM) Results

TEM micrographs of meso-Fe_2O_3 and meso-Co_3O_4 NPs used in the study are shown in Figures 9 and 10, respectively. In TEM micrographs, it is seen that the nanoparticles have a spherical morphology and spongy structure. This confirms the mesoporous structure of the particles. The advantage of these structures is that their catalytic efficiency increases due to their large surface area. Particle size analyses show that the average grain sizes of meso-Fe_2O_3 and meso-Co_3O_4 NPs are in the range of 21.37-64.15 nm and 164.65 nm, respectively.

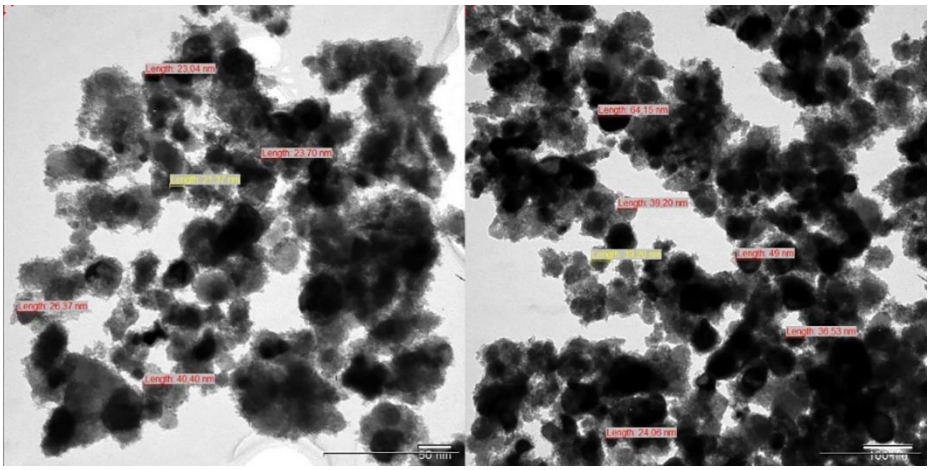

Figure 9: TEM images of meso-Fe_2O_3 NPs.

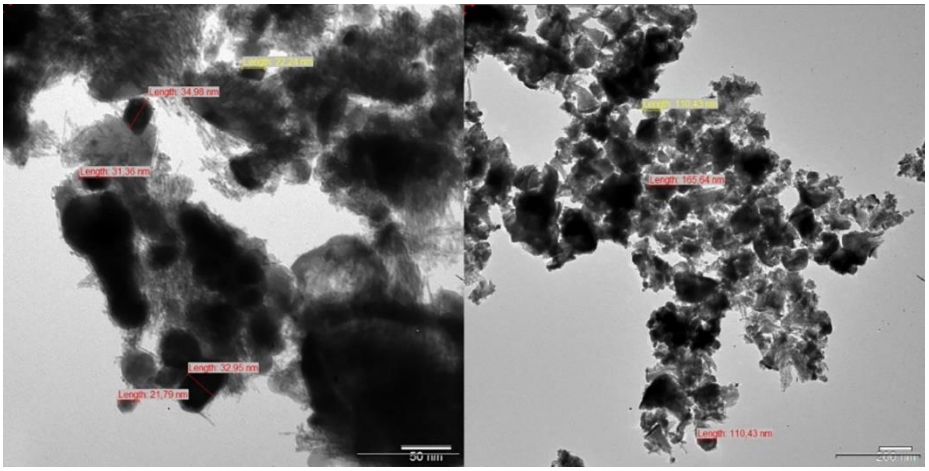

Figure 10: TEM images of meso-Co_3O_4 NPs.

3.2. AD studies

3.2.1. Chemical content analysis

In addition to the type of raw material used in biogas production (cattle, buffalo, etc.), parameters such as dry matter content, volatile solids, nitrogen, crude protein, and crude fat ratio are also important. Chemical analyses of organic feces were performed, and the results are given in Table 1.

Table 1: Chemical composition of feces.

Parameters	Feces (%)
Dry matter	8.16
Volatile solids	6.75
Ash	1.24
Total nitrogen (TKN)	1.86
Crude protein	11.63
Crude fat	1.67
pH	7.35

An important factor affecting biogas production is the solids rate, and the ideal rate for solids concentration has been reported as 7%–9% (31). In this study, the dry solids (DM) rate was calculated at 8.16%, and the ideal solids rate was achieved.

The Biogas production process comprises different stages and each stage encompasses numerous microbial flora to generate methane gas (32-33). Foremost, the mechanism of this process depends on the hydrolysis of complex organic material such as carbohydrates, lipids, and proteins, and convert them into solubilized, simple, and monomeric forms of sugar, fatty acids, and amino acids by hydrolytic enzymes produced by most of *Firmicutes* and *Bacteroides* phyla such as *clostridium* (34). Acidogenesis was followed by hydrolysis as an intermediatory step by acidogenic bacteria such as A*dvenella faeciporci, Alkalitalea saponilacus, Bacteroides caccae, Bifidobacterium animalis,* and *Cloacibacillus porc*orum etc. The solubilized product after hydrolysis was converted into alcohol and volatile fatty acids (35). Later on, further catabolism took place by acetogenic bacteria such as *Anaerovorax odorimutans, Hydrogenophaga carboriunda,* and *Macellibacteroides* fermentans, etc, which convert alcohols and volatile fatty acids into acetate and hydrogen (H_2) by organic acid and CO_2 known as acetogenesis. The final step in gas production is methanogenesis which refers to the production of methane from acetate, hydrogen (H_2), and CO_2 by special types of microbes (36). These methanogenic archaeas are categorized as hydrogenotrophic, acetoclastic, and methylotrophic, which utilized H_2 and formate, acetate, and methyl-containing compounds such as methyl sulfate, methylamines, and methanol respectively to produce methane CH_4 (37). During the process of production of clean energy, these above-mentioned four different groups of bacteria and archaea cooperate and strictly depend on each other to complete this cycle. However, to enhance the production of biogas,

nanoparticles are used to develop microbes-to-microbes communication during catalytic reactions. Nanoparticles play an important role by rapidly donating or accepting electrons by direct interspecies electron transfer (DIET) (38) or mediated interspecies electron transfer (MIET) mechanism (39). However, studies on DIET showed that lag time decreased the level of hydraulic retention time and increased the stage of methanogenesis to enhance the yield of biogas by improving the CH_4 purity and lowering the inhibitor resistance between microbes. In addition, it was found that the addition of metallic nanoparticles activates hydrogenotrophic methanogens and hydrogen-producing bacteria during methanogenesis, which significantly optimize traditional anaerobic digestion into a well-established energy production technology by enhancing CH_4 generation via CO_2 reduction at the electron acceptor step supported by methanogenic archaea (40, 41).

During the biogas production process, heavy metals, minerals, and detergents have toxic effects on the growth of microorganisms depending on their concentration. Low concentrations of ammonium, calcium, sodium, potassium, magnesium, and sulfur contribute to the proliferation of microorganisms. Likewise, chromium, copper, iron, etc. while heavy metals contribute to the development of microorganisms at very low levels, they have a toxic effect at high levels and reduce methane production efficiency. It has been reported that the use of Fe_3O_4, especially magnetic metal oxide, as a catalyst, increases biogas yield (42). It has been reported that the activity of autotrophic bacteria increases in the presence of a magnetic field between small magnetic NPs [43]. The slower proliferation of autotrophic bacteria is important for their growth and enrichment in the reactor. It has also been noted that interactions between magnetic NPs can involve activated sludge to create an anoxic environment favored by heterotrophic bacteria and eventually increase their activity [44]. The stimulatory effects of Fe_3O_4 NPs are attributed to the cellular uptake of NPs in methanogens and their association with metabolic intermediates and enzyme activity involved in manure hydrolysis, acidification, and methanation. It has also been reported that the shape and size of nanoparticles have an impact on nanoparticle-cell interactions and cellular uptake [45]. Cellular uptake of spherical nanoparticles with uniform particle size distribution is 500% higher than rod-shaped nanoparticles because the membrane wrapping time is longer for longer particles. Nanoparticle size strongly affects membrane receptor binding, activation, and protein expression [46]. Based on the literature, 0.3 g of catalyst was used in this study (15). The volume of biogas produced without using a catalyst was measured as 1.060 L/kg on the 20th day. The biogas volume obtained when a 0.3 g/L catalyst was used was determined to be 1.360 L/kg for γ-Fe_2O_3, 1.390 L/kg for meso-Fe_2O_3 and 625-1.250 L/kg for Co_3O_4. These results showed that the magnetic nanoparticles used led to increased anaerobic digestion and therefore higher methane production and organic matter processing. It has also been reported that the release of iron ions from magnetic NPs may be responsible for the increased bacterial activities [47]. In this study, γ-Fe_2O_3, meso-Fe_2O_3 and meso-Co_3O_4 magnetic nanoparticles used as catalysts cause the release of iron and cobalt ions into the reactor. This situation is also compatible with the literature [47].

3.2.2. Methane analysis in biogas

The methane amounts in the biogas content obtained without catalyst and with catalyst (γ-Fe_2O_3, Meso-Fe_2O_3, and Meso-Co_3O_4) in the biodigester are given in Table 2.

Table 2: Methane amounts in biogas content.

Sample	Methane (%)
- Fe_2O_3	85.3
Meso- Fe_2O_3	85.7
Meso-Co_3O_4	83.4
Without catalyst	75.4

An increase in methane production was observed when the catalyst was used under the same experimental conditions. This increase was determined as 9.9%, 10.3%, and 8% for γ-Fe_2O_3, Meso-Fe_2O_3 and Meso-Co_3O_4 catalysts, respectively. The different effects of γ-Fe_2O_3 and Meso-Fe_2O_3 catalysts under the same conditions can be explained by the increase in the surface area of the mesoporous structure.

4. CONCLUSION

It is important to utilize watery animal feces on cattle farms by turning them into products. Especially biogas production is a good alternative to meet the increasing energy need. The biogas obtained can be used for heating purposes as well as for electricity generation. Burdur province is at the forefront of the livestock sector, especially with dairy cattle farming, and ranks first in Türkiye in terms of the average amount of milk obtained from an animal. To avoid wasting hydrocarbons, Burdur province must increase the number of facilities where farm wastes are used and converted into methane gas.

In this study, a laboratory-scale biodigester was designed to produce biogas from cattle feces taken from Burdur Mehmet Akif Ersoy University Cattle Farm and was produced as a prototype for a local company. Structural characterizations of the catalysts were carried out using FT-IR and XRD techniques. XRD powder patterns show that γ-Fe_2O_3 is formed in a maghemite structure in a tetragonal crystal system with P43212(96) space group (PDF card no: 00-025-1402). The mesoporous Fe_2O_3 nanoparticles are formed in the hematite structure in a rhombohedral crystal structure and an R-3c (167) crystal system (PDF Card no: 00-033-0664). Co_3O_4 nanoparticles are formed in a cubic crystal system with an Fd-3m space group (227) (PDF card no: 00-042-1467). The average particle sizes of nanoparticles were determined to be in the range of 20-165 nm. The biodigester was kept at a constant temperature of 35 °C for 20 days, and the volume of gas released was measured. The obtained biogas in the biodigester was absorbed into the adsorbent material (activated carbon) and analyzed with the headspace-GC-MS combined system. In this study, it

was observed that spherical γ-Fe_2O_3, meso-Fe_2O_3 and meso-Co_3O_4 magnetic nanoparticles used as nanocatalysts improved biogas and methane production. The amount of methane in the biogas obtained without using a catalyst was found to be 75.4%. When γ-Fe_2O_3, meso-Fe_2O_3, and meso-Co_3O_4 nanoparticles were used as catalysts, the methane ratio was calculated as 85.3, 85.7, and 83.4, respectively. The results obtained from the study showed that in addition to γ-Fe_2O_3 used as a catalyst in biogas production, meso-Fe_2O_3 and meso-Co_3O_4 nanoparticles also have the potential to be used for this purpose.

5. CONFLICT OF INTEREST

The authors declare no conflict of interest.

6. ACKNOWLEDGMENTS

This study was supported by Burdur Mehmet Akif Ersoy University Scientific Research Projects Coordinatorship with Project No: 0715-MP-21. The authors also would like to thank Assoc. Prof. Dr. Ruken Esra Demirdöğen for her valuable contribution.

7. REFERENCES

1. Kona A, Bertoldi P, Kılkış Ş. Covenant of Mayors: Local Energy Generation, Methodology, Policies and Good Practice Examples. Energies [Internet]. 2019 Mar 13;12(6):985. Available from: <URL>.

2. Dabe SJ, Prasad PJ, Vaidya AN, Purohit HJ. Technological pathways for bioenergy generation from municipal solid waste: Renewable energy option. Environ Prog Sustain Energy [Internet]. 2019 Mar 25;38(2):654–71. Available from: <URL>.

3. Mikalauskiene A, Štreimikis J, Mikalauskas I, Stankūnienė G, Dapkus R. Comparative Assessment of Climate Change Mitigation Policies in Fuel Combustion Sector of Lithuania and Bulgaria. Energies [Internet]. 2019 Feb 7;12(3):529. Available from: <URL>.

4. Holdmann GP, Wies RW, Vandermeer JB. Renewable Energy Integration in Alaska's Remote Islanded Microgrids: Economic Drivers, Technical Strategies, Technological Niche Development, and Policy Implications. Proc IEEE [Internet]. 2019 Sep;107(9):1820–37. Available from: <URL>.

5. Viancelli A, Schneider TM, Demczuk T, Delmoral APG, Petry B, Collato MM, et al. Unlocking the value of biomass: Exploring microbial strategies for biogas and volatile fatty acids generation. Bioresour Technol Reports [Internet]. 2023 Sep;23:101552. Available from: <URL>.

6. Havukainen J, Uusitalo V, Niskanen A, Kapustina V, Horttanainen M. Evaluation of methods for estimating energy performance of biogas production. Renew Energy [Internet]. 2014 Jun;66:232–40. Available from: <URL>.

7. Yusuf MOL, Ify NL. The effect of waste paper on the kinetics of biogas yield from the co-digestion of cow dung and water hyacinth. Biomass and Bioenergy [Internet]. 2011 Mar;35(3):1345–51. Available from: <URL>.

8. Koniuszewska I, Korzeniewska E, Harnisz M, Czatzkowska M. Intensification of biogas production using various technologies: A review. Int J Energy Res [Internet]. 2020 Jun 25;44(8):6240–58. Available from: <URL>.

9. Barozzi M, Contini S, Raboni M, Torretta V, Casson Moreno V, Copelli S. Integration of Recursive Operability Analysis, FMECA and FTA for the Quantitative Risk Assessment in biogas plants: Role of procedural errors and components failures. J Loss Prev Process Ind [Internet]. 2021 Jul;71:104468. Available from: <URL>.

10. Shakil Hussain SM, Kamal MS, Hossain MK. Recent Developments in Nanostructured Palladium and Other Metal Catalysts for Organic Transformation. J Nanomater [Internet]. 2019 Oct 20;2019:1562130. Available from: <URL>.

11. Srivastava N, Srivastava KR, Bantun F, Mohammad A, Singh R, Pal DB, et al. Improved production of biogas via microbial digestion of pressmud using CuO/Cu_2O based nanocatalyst prepared from pressmud and sugarcane bagasse waste. Bioresour Technol [Internet]. 2022 Oct;362:127814. Available from: <URL>.

12. Ribeaucourt D, Bissaro B, Guallar V, Yemloul M, Haon M, Grisel S, et al. Comprehensive Insights into the Production of Long Chain Aliphatic Aldehydes Using a Copper-Radical Alcohol Oxidase as Biocatalyst. ACS Sustain Chem Eng [Internet]. 2021 Mar 29;9(12):4411–21. Available from: <URL>.

13. Ozyilmaz E, Alhiali A, Caglar O, Yilmaz M. Preparation of regenerable magnetic nanoparticles for cellulase immobilization: Improvement of enzymatic activity and stability. Biotechnol Prog [Internet]. 2021 Mar 22;37(4):e3145. Available from: <URL>.

14. Watanabe T, Takawane S, Baba Y, Akaiwa J, Kondo A, Ohba T. Superior Thermal Stability and High Photocatalytic Activity of Titanium Dioxide Nanocatalysts in Carbon Nanotubes. J Phys Chem C [Internet]. 2023 Aug 31;127(34):16861–9. Available from: <URL>.

15. Gómez-Gualdrón DA, McKenzie GD, Alvarado JFJ, Balbuena PB. Dynamic Evolution of Supported Metal Nanocatalyst/Carbon Structure during Single-Walled Carbon Nanotube Growth. ACS Nano [Internet]. 2012 Jan 24;6(1):720–35. Available from: <URL>.

16. Bhanja P, Bhaumik A. Materials with Nanoscale Porosity: Energy and Environmental Applications. Chem Rec [Internet]. 2019 Feb 2;19(2–3):333–46. Available from: <URL>.

17. Zhou L, Zheng J, Ye E, Liu Y, He C. Nanocatalysis with sustainability. In: Li Z, Zheng J, Ye E, editors. Nanoscience and Nanotechnology Series, Sustainable Nanotechnology [Internet]. London:

10.1039/9781839165771; 2022. p. 220–54. Available from: <URL>.

18. Touchy AS, Siddiki SMAH. Green Chemical Synthesis in the Presence of Nanoparticles as Catalysts. In: Singh NB, Susan ABH, Chaudhary RG, editors. Emerging Applications of Nanomaterials. Millersville: Materials Research Forum LLC; 2023. p. 42–74.

19. Bharathi P, Dayana R, Rangaraju M, Varsha V, Subathra M, Gayathri, et al. Biogas Production from Food Waste Using Nanocatalyst. R L, editor. J Nanomater [Internet]. 2022 Jul 31;2022:7529036. Available from: <URL>.

20. Awogbemi O, Kallon DV Von. Recent advances in the application of nanomaterials for improved biodiesel, biogas, biohydrogen, and bioethanol production. Fuel [Internet]. 2024 Feb;358:130261. Available from: <URL>.

21. Jayanthi SA, Nathan DMGT, Jayashainy J, Sagayaraj P. A novel hydrothermal approach for synthesizing α-Fe_2O_3, γ-Fe_2O_3 and Fe_3O_4 mesoporous magnetic nanoparticles. Mater Chem Phys [Internet]. 2015 Jul;162:316–25. Available from: <URL>.

22. Li D, Wu X, Xiao T, Tao W, Yuan M, Hu X, et al. Hydrothermal synthesis of mesoporous Co_3O_4 nanobelts by means of a compound precursor. J Phys Chem Solids [Internet]. 2012 Feb;73(2):169–75. Available from: <URL>.

23. Zhang L, Papaefthymiou GC, Ying JY. Synthesis and Properties of γ-Fe_2O_3 Nanoclusters within Mesoporous Aluminosilicate Matrices. J Phys Chem B [Internet]. 2001 Aug 1;105(31):7414–23. Available from: <URL>.

24. Demir Ö, Ateş N. Manyetik Nanopartiküllerin Anaerobik Çürütücüde Biyogaz Üretimi Üzerine Etkileri. Çukurova Üniversitesi Mühendislik Fakültesi Derg [Internet]. 2021 Aug 16;36(2):283–96. Available from: <URL>.

25. Yılmazer M, Seçilmiş H. Gaz kromatografisi headspace sistemi ile süt ürünlerinde bazı aroma bileşenlerinin analizi. In: Türkiye 9 Gıda Kongresi. 2006. p. 24–6.

26. Omoniyi TE, Olorunnisola AO. Experimental characterisation of bagasse biomass material for energy production. Int J Eng Technol. 2014;4(10):582–9. Available from: <URL>.

27. Beutler M, Wiltshire KH, Meyer B, Moldaenke C, Luring C, Meyerhofer M, Hansen UP. APHA (2005), Standard Methods for the Examination of Water and Wastewater, Washington DC: American Public Health Association. 2014;

28. Huang Y, Zhang D, Oshita K, Takaoka M, Ying M, Sun Z, et al. Crude oil recovery from oily sludge using liquefied dimethyl ether extraction: A comparison with conventional extraction methods. Energy and Fuels [Internet]. 2021 Nov 4 [cited 2024 Feb 27];35(21):17810–9. Available from: <URL>.

29. Parsianpour E, Gholami M, Shahbazi N, Samavat F. Influence of thermal annealing on the structural and optical properties of maghemite (γ-Fe_2O_3) nanoparticle thin films. Surf Interface Anal [Internet]. 2015 May 12;47(5):612–7. Available from: <URL>.

30. Mishra D, Arora R, Lahiri S, Amritphale SS, Chandra N. Synthesis and characterization of iron oxide nanoparticles by solvothermal method. Prot Met Phys Chem Surfaces [Internet]. 2014 Sep 12;50(5):628–31. Available from: <URL>.

31. Jagadale AD, Kumbhar VS, Lokhande CD. Supercapacitive activities of potentiodynamically deposited nanoflakes of cobalt oxide (Co_3O_4) thin film electrode. J Colloid Interface Sci [Internet]. 2013 Sep;406:225–30. Available from: <URL>.

32. Wang S, Jena U, Das KC. Biomethane production potential of slaughterhouse waste in the United States. Energy Convers Manag [Internet]. 2018 Oct;173:143–57. Available from: <URL>.

33. Wang P, Wang H, Qiu Y, Ren L, Jiang B. Microbial characteristics in anaerobic digestion process of food waste for methane production–A review. Bioresour Technol [Internet]. 2018 Jan;248:29–36. Available from: <URL>.

34. Nguyen D, Khanal SK. A little breath of fresh air into an anaerobic system: How microaeration facilitates anaerobic digestion process. Biotechnol Adv [Internet]. 2018 Nov;36(7):1971–83. Available from: <URL>.

35. Hendriks ATWM, van Lier JB, de Kreuk MK. Growth media in anaerobic fermentative processes: The underestimated potential of thermophilic fermentation and anaerobic digestion. Biotechnol Adv [Internet]. 2018 Jan;36(1):1–13. Available from: <URL>.

36. Li Y, Chen Y, Wu J. Enhancement of methane production in anaerobic digestion process: A review. Appl Energy [Internet]. 2019 Apr;240:120–37. Available from: <URL>.

37. Venkiteshwaran K, Bocher B, Maki J, Zitomer D. Relating Anaerobic Digestion Microbial Community and Process Function : Supplementary Issue: Water Microbiology. Microbiol Insights [Internet]. 2015 Jan 20;8(S2):37–44. Available from: <URL>.

38. Bai X, Zong R, Li C, Liu D, Liu Y, Zhu Y. Enhancement of visible photocatalytic activity via Ag@C3N4 core–shell plasmonic composite. Appl Catal B Environ [Internet]. 2014 Apr;147:82–91. Available from: <URL>.

39. Appels L, Baeyens J, Degrève J, Dewil R. Principles and potential of the anaerobic digestion of waste-activated sludge. Prog Energy Combust Sci [Internet]. 2008 Dec;34(6):755–81. Available from: <URL>.

40. Cuetos MJ, Martinez EJ, Moreno R, Gonzalez R, Otero M, Gomez X. Enhancing anaerobic digestion of poultry blood using activated carbon. J Adv Res

[Internet]. 2017 May;8(3):297–307. Available from: <URL>.

41. Tsapekos P, Alvarado-Morales M, Tong J, Angelidaki I. Nickel spiking to improve the methane yield of sewage sludge. Bioresour Technol [Internet]. 2018 Dec;270:732–7. Available from: <URL>.

42. Abdelsalam E, Samer M, Attia YA, Abdel-Hadi MA, Hassan HE, Badr Y. Influence of zero valent iron nanoparticles and magnetic iron oxide nanoparticles on biogas and methane production from anaerobic digestion of manure. Energy [Internet]. 2017 Feb;120:842–53. Available from: <URL>.

43. Łebkowska M, Rutkowska-Narożniak A, Pajor E, Pochanke Z. Effect of a static magnetic field on formaldehyde biodegradation in wastewater by activated sludge. Bioresour Technol [Internet]. 2011 Oct;102(19):8777–82. Available from: <URL>.

44. Ni SQ, Ni J, Yang N, Wang J. Effect of magnetic nanoparticles on the performance of activated sludge treatment system. Bioresour Technol [Internet]. 2013 Sep;143:555–61. Available from: <URL>.

45. Verma A, Stellacci F. Effect of Surface Properties on Nanoparticle–Cell Interactions. Small [Internet]. 2010 Jan 4;6(1):12–21. Available from: <URL>.

46. Jiang W, Kim BYS, Rutka JT, Chan WCW. Nanoparticle-mediated cellular response is size-dependent. Nat Nanotechnol [Internet]. 2008 Mar 2;3(3):145–50. Available from: <URL>.

47. Liu Y, Zhang Y, Quan X, Chen S, Zhao H. Applying an electric field in a built-in zero valent iron – Anaerobic reactor for enhancement of sludge granulation. Water Res [Internet]. 2011 Jan;45(3):1258–66. Available from: <URL>.